



Lead-containing Beta zeolites as versatile Lewis acid catalysts for the aminolysis of epoxides

Yuchao Chai^{a,b}, Linjun Xie^{a,b}, Zhiyang Yu^c, Weili Dai^{a,b}, Guangjun Wu^{a,b}, Naijia Guan^{a,b}, Landong Li^{a,b,*}

^a School of Materials Science and Engineering & National Institute for Advanced Materials, Nankai University, Tianjin 300350, China

^b Key Laboratory of Advanced Energy Materials Chemistry of Ministry of Education, Collaborative Innovation Center of Chemical Science and Engineering, Nankai University, Tianjin 300071, China

^c School of Materials Science and Engineering, Xiamen University of Technology, Xiamen 361024, China

ARTICLE INFO

Keywords:

Lead
BEA
Lewis acid
Aminolysis
Epoxide

ABSTRACT

Pb-Beta, a heteroatom zeolite containing out-size atoms of lead, has been successfully prepared via a scalable post-synthesis strategy composed of dealumination of H-Beta to create associated silanol and subsequent dry impregnation of the resulting Si-Beta with lead nitrate. The incorporated lead species exist in the form of well-isolated tetra-coordinated Pb²⁺ ions with open configurations, as revealed by the characterization results from high angle annular dark field scanning transmission electron microscopy (HAADF-STEM), UV-Vis, X-ray photoelectron spectroscopy (XPS) and ²⁹Si solid-state magic angle spinning nuclear magnetic resonance (MAS NMR) spectroscopy. Sufficient Lewis acid sites with moderate acid strength are created by lead incorporation into zeolite framework, as confirmed by the temperature-programmed desorption of ammonia (NH₃-TPD). The as-prepared Pb-Beta Lewis acid zeolites exhibit remarkable catalytic activity in the ring-opening aminolysis of epoxides to β-amino alcohols with high regio-selectivity. The presence of wide-open lead sites can promote the simultaneous activation of epoxide and amine substrates and, therefore, catalyze the aminolysis of epoxides with strong basic amines, e.g. butylamine.

1. Introduction

Heteroatoms substituted zeolites, known as well-defined single-site Lewis acid catalysts, have attracted considerable attention due to their widespread applications in sustainable chemistry and eco-friendly chemical processes [1–6]. Generally, heteroatom substituted zeolites can be prepared via direct hydrothermal synthesis or post-synthesis strategy. The direct hydrothermal synthesis unavoidably involves the use of hazardous raw materials and long time-scale to realize full crystallization, and sometimes a lack of reproducibility is claimed [7,8]. In contrast, the post-synthesis strategy offers an effective and versatile approach to various heteroatom substituted zeolites, even to hierarchically structured zeolites [9,10]. Beta zeolite, with large 12-ring channels (BEA: [100] 0.66 × 0.67 nm ↔ [001] 0.56 × 0.56 nm), is a good precursor for post-synthesis modifications, in which Beta zeolite is partially or fully dealuminated to generate vacant sites for heteroatom substitution [11,12]. The incorporation of heteroatom into framework positions can significantly change the intrinsic acidity of Beta zeolite, i.e. creation of Lewis acid sites with different configurations and different strength [13–16].

Since the ionic radius of heteroatoms (M), e.g. Ti⁴⁺ (0.61 Å), Zr⁴⁺ (0.72 Å), and Sn⁴⁺ (0.71 Å) are generally larger than the pristine Al³⁺ (0.54 Å) or the silicate matrix (0.41 Å for Si⁴⁺), the heteroatoms are difficult to be fully incorporated into vacant sites of dealuminated-Beta zeolite to obtain M sites with closed configuration ([M(OSi)₄], abbreviated as close site), and a certain amount of M sites with open configurations ([M(OSi)₃(OH)], [M(OSi)₂(OH)₂] or [M(OSi)(OH)₃], abbreviated as open sites) would be expected (Chart 1) [12,15,17]. Zr- and Sn-Beta with larger ionic radius of heteroatoms should have more open sites with respect to Ti-Beta [12,18,19]. Recently, featured by their high catalytic activity in a variety of reactions, open sites in Ti-, Zr-, and Sn-Beta have drawn particular interests. For instance, Ratnasamy et al. [20] reported that the creation of open sites [Ti(OSi)₃(OH)] in Ti-Beta could significantly facilitate the catalytic oxidation of organic substrate by H₂O₂. Similar results were reported by Thomson et al. [21] and Lamberti et al. [22] in the epoxidation of propylene reaction using TS-1 with open sites as catalysts. Very recently, Ivanova et al. [19,23] provided experimental evidence for the open and closed Lewis acid sites in Zr-Beta zeolite and confirmed that

* Corresponding author. School of Materials Science and Engineering & National Institute for Advanced Materials, Nankai University, Tianjin 300350, China.
E-mail address: lild@nankai.edu.cn (L. Li).

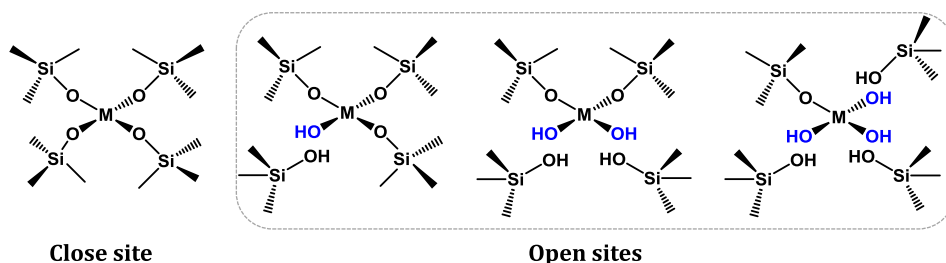


Chart 1. Modes of close site and open sites.

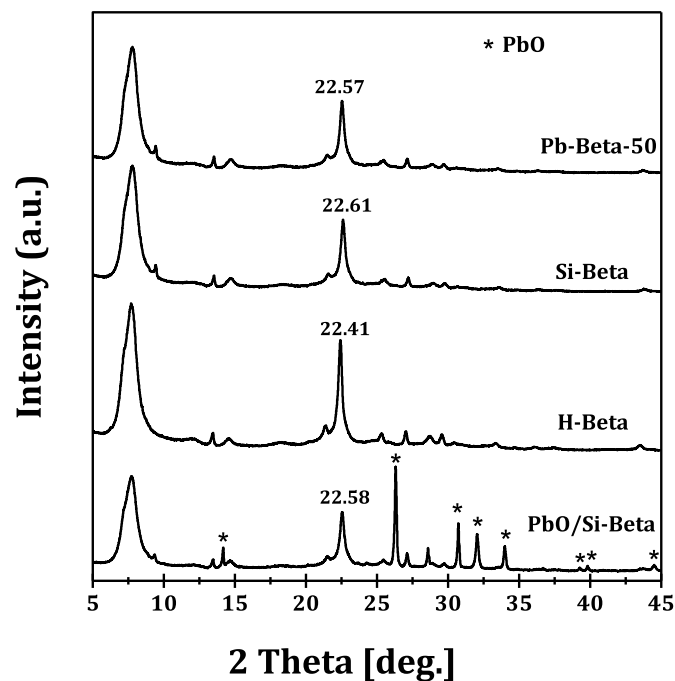


Fig. 1. XRD patterns of selected zeolite samples.

Table 1
Textural properties of H-Beta, Si-Beta, and M-Beta.

Catalyst	Si/Al ^a	Si/M ^a	Surface area ^b (m ² g ⁻¹)	Micropore volume ^c (cm [3] g ⁻¹)
H-Beta	13.5	/	594	0.232
Si-Beta	> 1800	/	652	0.257
Pb-Beta-100	> 1800	98.5	562	0.218
Pb-Beta-50	> 1800	50.8	544	0.215
Pb-Beta-30	> 1800	34.2	552	0.217
Sn-Beta-50	> 1800	51.3	580	0.200
Zr-Beta-50	> 1800	48.9	573	0.197
Ti-Beta-50	> 1800	49.1	575	0.198

^a Determined by XRF.

^b Specific surface area obtained by BET method.

^c Calculated from *t*-plot.

the open sites [Zr(OSi)₃(OH)] was beneficial for the conversion of ethanol to butadiene. Moreover, Gounder et al. [15] demonstrated that open Sn sites served as the dominant active sites in Sn-Beta for glucose-fructose isomerization via intramolecular 1,2-hydride shift. According to these reports, open Lewis acid sites from large framework heteroatoms may contribute to more active catalytic sites and better accessibility for substrate molecules in various chemical processes.

Generally, the Lewis acid strength of M-Beta zeolites is dominated by the natural attributes of heteroatoms in the sequence of Sn-Beta > Zr-Beta > Ti-Beta [24–27]. The strength of M-Beta Lewis acids

will directly influence their catalytic behaviors in various reactions and, in turn, M-Beta zeolite with specific Lewis acidity can be optimized for a designated reaction. For example, Sn-Beta can catalyze the chemoselective Baeyer-Villiger oxidation of ketones and aldehydes, whereas Ti- or Zr-Beta with lower Lewis acid strength cannot [5,17]. On the other hand, Ti-, Zr- and Sn-Beta are all active solid Lewis acid catalysts in the Meerwein-Ponndorf-Verly reduction of cyclohexanone with 2-butanol, but their activities are somewhat different [17,28,29]. In this context, the precise design of M-Beta zeolite catalyst with controllable Lewis acidity is urgently desired, especially for the reactions that are sensitive to the strength of Lewis acid sites.

Aminolysis of epoxides provides an efficient route to β-amino alcohols, which are the versatile intermediates for the synthesis of various biologically active products and pesticides [30,31]. The ring-open of epoxides with amines is very sensitive to the Lewis acid strength of catalysts, as weak Lewis acid sites are not sufficient to activate the epoxide substrates while too strong Lewis acid sites will be covered by strongly bonded amine molecules to hinder their reaction with epoxides [32,33]. Zirconosilicate zeolites with moderate Lewis acid, e.g. Zr-Beta and Zr-MFI, have been reported as promising candidates for this type of reaction [26,34]. However, Zr-containing zeolites are not general catalysts, especially when amines with high basicity, e.g. butylamine, are employed as reactants.

Inspired by the above-mentioned achievements and motivated by current challenges, we herein report the construction of lead-containing Beta zeolites, i.e. Pb-Beta, via a post-synthesis strategy. Pb is generally recognized as a deactivating component or modifier rather than active component in solid catalysts. To the best of our knowledge, this is the first time to incorporate outside heteroatom Pb (1.2 Å) into zeolite framework. Upon Pb incorporation, open Lewis acid sites are created, which can efficiently catalyze the ring-opening aminolysis of epoxides, even using butylamine with high basicity as a reactant.

2. Experiment

2.1. Sample preparation

Commercial H-Beta with an $n_{\text{Si}}/n_{\text{Al}}$ of 13.5 (Nankai University) was used as the starting material for synthesizing metal incorporating Beta zeolites. Pb-Beta catalysts were prepared via a two-step postsynthesis procedure consisting of the dealumination of the parent H-Beta to get the Si-Beta material and subsequent incorporation of Pb into the Si-Beta framework. Briefly, parent H-Beta was stirred in a 13 mol L⁻¹ nitric acid aqueous solution (20 mL g_{zeolite}⁻¹) at 373 K overnight to obtain a dealuminated Si-Beta. The slurry was filtered, washed with distilled water until pH = 7, and then dried at 353 K for 12 h. Afterwards, 1.0 g Si-Beta host zeolite was finely impregnated with appropriate amount of Pb(NO₃)₂ in 100 mL H₂O, and dried at 353 K to achieve an intimate mixture powder with the $n_{\text{Si}}/n_{\text{Pb}}$ ratio of 30 (Pb-Beta-30), 50 (Pb-Beta-50), 100 (Pb-Beta-100), respectively. The solid mixture was put into a tubular reactor, then sealed and heated to 823 K for 6 h with 5 K min⁻¹ heating rate to obtain Pb-containing zeolite material.

For reference, as described in our previous reports, Ti-, Zr- and Sn-Beta samples were also prepared via similar procedures, with

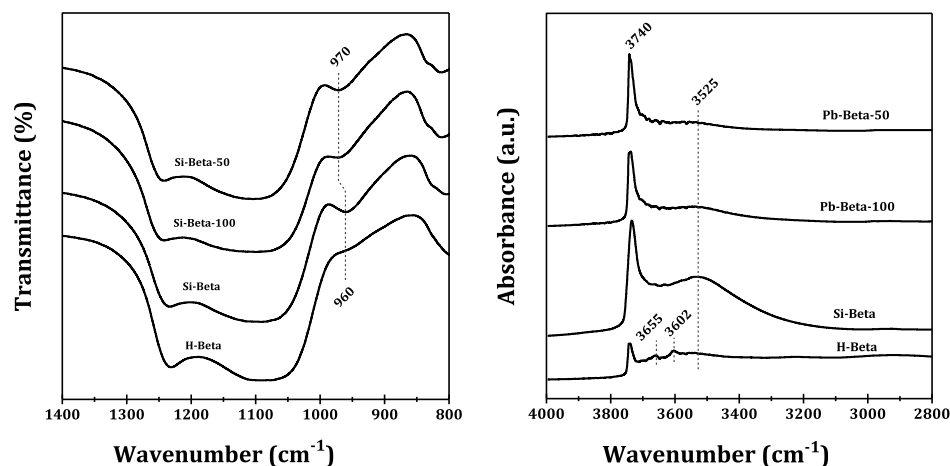
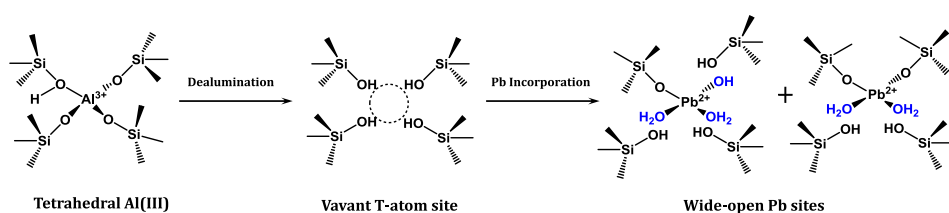


Fig. 2. FTIR transmittance spectra of the skeletal vibrations (left) and FTIR diffuse reflectance spectra in the hydroxyl stretching vibration regions (right) of selected zeolite samples.



Scheme 1. Schematic representation of the incorporation of tetrahedrally coordinated Pb^{2+} species into Beta zeolite.

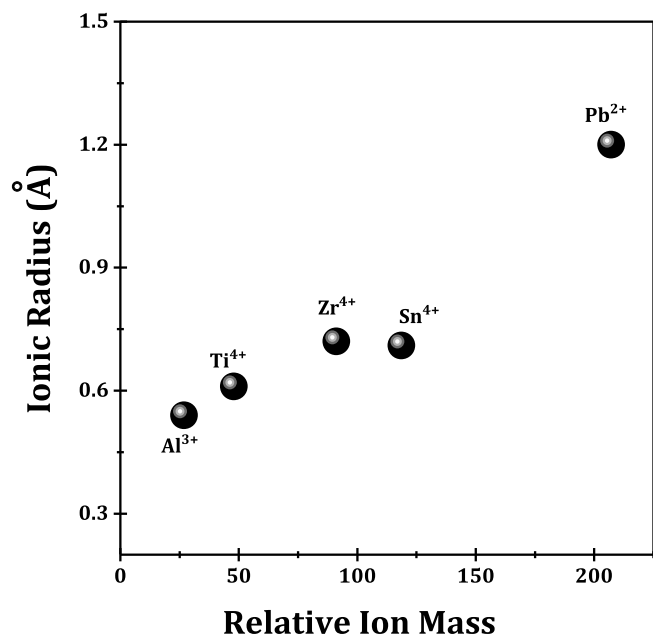


Fig. 3. The ionic radius of selected heteroatoms.

organometallic precursors Cp_2TiCl_2 , Cp_2ZrCl_2 and $(\text{CH}_3)_2\text{SnCl}_2$, respectively. In addition, the Si-Beta supported lead monoxide ($\text{PbO}/\text{Si-Beta}$) were prepared via mechanical mixing of Si-Beta with PbO species, followed by calcination at 823 K for 12 h.

2.2. Characterization techniques

The chemical compositions of zeolite samples were analyzed by Philips PW2424 X-ray fluorescence spectroscopy (XRF).

The X-ray diffraction (XRD) patterns of zeolite samples were recorded on a Bruker D8 diffractometer using $\text{Cu-K}\alpha$ radiation ($\lambda = 0.1541 \text{ nm}$) at a scanning rate of $6^\circ/\text{min}$ in the region of $2\theta = 5\text{--}50^\circ$.

The surface areas of zeolite samples were determined by argon adsorption/desorption isotherms at 87 K collected on a Quantachrome iQ-MP gas adsorption analyzer. The total surface area was calculated via the Brunauer Emmett Teller (BET) equation and the micropore size distribution was determined using the t-plot method.

Scanning electron microscopy (SEM) images of samples were obtained on a Hitachi S-4800 microscope.

Diffuse reflectance infrared Fourier transform (FTIR) spectra of zeolite samples were taken on a Bruker Tensor 27 spectrometer with 128 scans at a resolution of 2 cm^{-1} . The samples were pre-treated in flowing He at 673 K for 1 h. The spectra were recorded in He against KBr as the background.

High angle annular dark field scanning transmission electron microscopy (HAADF-STEM) images were acquired on a FEI Talos electron microscope. Since zeolite crystals are quite sensitive to electron beam, under HAADF mode, we reduced the probe size to 10 (beam current: $\sim 16 \text{ pA}$) for high quality HAADF imaging. Mapping the elemental distribution of zeolite crystals was conducted under HAADF-STEM mode using a FEI built-in energy dispersive spectrum (EDS) software with drift correction applied.

Diffuse reflectance ultraviolet-visible (UV-vis) spectra of the dehydrated zeolite samples were measured in the range of 200–1000 nm on a PerkinElmer Lambda 750 UV-Vis-NIR spectrophotometer.

X-ray photoelectron spectra (XPS) of materials were recorded on a Thermo Scientific ESCALAB 250Xi spectrometer with a monochromatic $\text{Al-K}\alpha$ X-ray source ($h\nu = 1486.6 \text{ eV}$) as the excitation source. Accurate binding energies ($\pm 0.1 \text{ eV}$) were determined with respect to the position of the adventitious C 1s peak at 284.8 eV.

Raman analysis was carried out with a Horiba Jobin Yvon Raman spectrometer and the spectra were obtained using the green line of an argon-ion laser (512.0 nm) in a micro-Raman configuration.

Solid-state magic angle spinning nuclear magnetic resonance (MAS NMR) experiments were performed on a Bruker Avance III 400WB spectrometer at resonance frequencies of 79.5 MHz for ^{29}Si NMR.

The experiments of temperature-programmed desorption of ammonia ($\text{NH}_3\text{-TPD}$) were performed on a Quantachrome ChemBet 3000 chemisorption instrument. In a typical experiment, the sample was saturated with 5% NH_3/He at 323 K and then purged with He at the

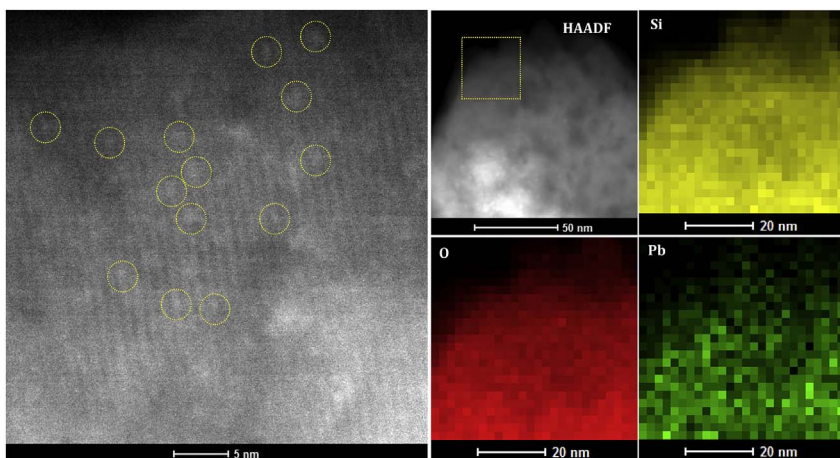


Fig. 4. HAADF-STEM image of Pb-Beta-50 and element mapping analysis (Si, O and Pb).

same temperature for 1 h to eliminate the physical absorbed ammonia. NH_3 -TPD profile was recorded in flowing He at a heating rate of $10^\circ\text{C}/\text{min}$ from 323 to 1073 K.

2.3. Catalytic evaluation

The aminolysis of epoxides were performed in a 25 mL round-bottom glass flask with a water bath under atmospheric pressure. In a typical experiment, 25 mg catalyst, 10 mmol epoxide, and 10 mmol amine were mixed vigorously using a magnetic stirrer. After the reaction, the liquid organic products were analyzed by gas chromatography (Shimadzu GC-2010) and gas chromatography-mass spectrometry (Shimadzu GCMS-QP2010 SE), both with a HP-5MS column ($30\text{ m} \times 0.25\text{ mm} \times 0.25\text{ }\mu\text{m}$; FID detector). n-Dodecane was used as an internal standard for quantification.

Recycling tests in the aminolysis of epoxides over Pb-Beta catalyst were conducted. In a typical experiment, the mixture after one reaction cycle (0.5 h) was centrifuged at 8000 rpm to deposit the solid catalyst, which was washed with CH_2Cl_2 and dried at 353 K for 12 h for next use directly.

3. Results and discussion

3.1. Incorporation of open-site Pb species into zeolite framework

The XRD patterns of the parent H-Beta and post-treated samples (Si-Beta and Pb-Beta) are collected and shown in Fig. 1. All samples exhibit similar diffraction peaks corresponding to typical BEA topology, ruling out the obvious collapse of zeolite framework during the dealumination and Pb incorporation (peaks at $\sim 9.44^\circ$ associated with defect sites in BEA zeolite). For Pb-Beta-50 (6.5 wt%), no diffraction peaks corresponding to lead oxides can be observed due to the high dispersion of Pb species, while the PbO/Si-Beta (6.5 wt%) exhibits clear diffraction peaks corresponding to PbO (JCPDF 72-0093). The well-preserved microporous BEA structure after dealumination and Pb incorporation is further confirmed by the argon physisorption (Fig. S1), in which similar typeIadsorption/desorption isotherms are observed for all samples.

Table 1 summarizes the physicochemical properties of H-Beta, Si-Beta, and Pb-Beta samples. All samples exhibit similar BET surface areas ($544\text{--}652\text{ m}^2\text{ g}^{-1}$) and micropore volumes ($0.215\text{--}0.257\text{ cm}^3\text{ g}^{-1}$), confirming the well preserved textural properties of Beta zeolite after dealumination and Pb incorporation. XRF analysis results reveal that, upon treatment with concentrated HNO_3 , the $n_{\text{Si}}/n_{\text{Al}}$ ratio of the parent H-Beta sharply increases from 13.5 to > 1800 of dealuminated Si-Beta, indicating the latter being essentially free of Al species. After the incorporation of Pb, the actual $n_{\text{Si}}/n_{\text{Pb}}$ ratio determined by XRF is quite

close to the target value at relatively low Pb loadings ($n_{\text{Si}}/n_{\text{Pb}} = 100, 50$). While at the highest Pb loading ($n_{\text{Si}}/n_{\text{Pb}} = 30$), the actual Pb loading is obviously lower ($n_{\text{Si}}/n_{\text{Pb}} = 34$), implying the supersaturation of the Pb incorporation and a loss of Pb species during the calcination process, which will be discussed in detail in the next section.

The SEM images of the H-Beta, Si-Beta, and Pb-Beta-50 are shown in Fig. S2. The small crystal grains (100–200 nm) with the similar morphology can be clearly observed for the three samples, excluding the possible morphology changes upon dealumination and Pb incorporation. Furthermore, the well-defined lattice fringes of Pb-Beta-50 can be observed in the high-resolution TEM image (Fig. S3), confirming that the crystal structure remains intact through post-synthesis modifications. Selected-area EDS analysis results indicate the existence of Pb elements (4.5 wt%), while the bulky PbO particles cannot be observed in the high-resolution TEM image, hinting well-isolated Pb species or even single Pb atoms associated with zeolite framework (vide infra).

The incorporation of metal ions into zeolite framework can be monitored by means of infrared spectroscopy [35]. Fig. 2 (left-chart) shows the FTIR transmittance spectra in the framework vibration region ($800\text{--}1400\text{ cm}^{-1}$) of the parent H-Beta and post-treated samples (hydrated). The new FTIR band center at 960 cm^{-1} appears for the Si-Beta sample by a deep dealumination of H-Beta with concentrated HNO_3 solution, while no obvious bands in the range of $900\text{--}1000\text{ cm}^{-1}$ can be detected for the H-Beta sample. The newly-formed band at 960 cm^{-1} is due to the presence of abundant silanols created by framework dealumination [36,37]. After the impregnation with $\text{Pb}(\text{NO}_3)_2$ and subsequent calcination, the IR band at 960 cm^{-1} disappears, indicating the interaction between Pb species and silanols. Meanwhile, a new FTIR band centered at 970 cm^{-1} occurs for the Pb-Beta zeolites due to the formation of hydroxyls bonded to Pb atoms [37,38]. This should indicate the formation of open Pb sites in Pb-Beta, since close Pb sites do not contain any hydroxyls. The evolution of hydroxyls during post-synthesis of Pb-Beta (all sample are dehydrated) are further analyzed by the DRIFT spectra (Fig. 2, right-chart). The parent H-Beta clearly exhibits several characteristic bands in hydroxyl stretching region [39,40]: isolated external Si-OH groups (3740 cm^{-1}), extra-framework Al-OH groups (3655 cm^{-1}) and bridging hydroxyls Si-OH-Al (3605 cm^{-1}). After the treatment of H-Beta zeolite with concentrated HNO_3 solution, for resulting Si-Beta sample, two bands at 3655 and 3605 cm^{-1} bands related to framework Al species disappear due to the complete removal of Al atoms from zeolite framework, as revealed by XRF analysis ($n_{\text{Si}}/n_{\text{Al}} > 1800$). Concurrently, the intensification of the band at 3740 cm^{-1} due to isolated internal Si-OH groups and the appearance of broad band centered at 3525 cm^{-1} due to associated Si-OH groups can be observed [40], indicating the formation of defect sites located at the vacant T sites of the dealuminated Si-Beta framework (Scheme 1, dealumination step). The subsequent incorporation of Pb

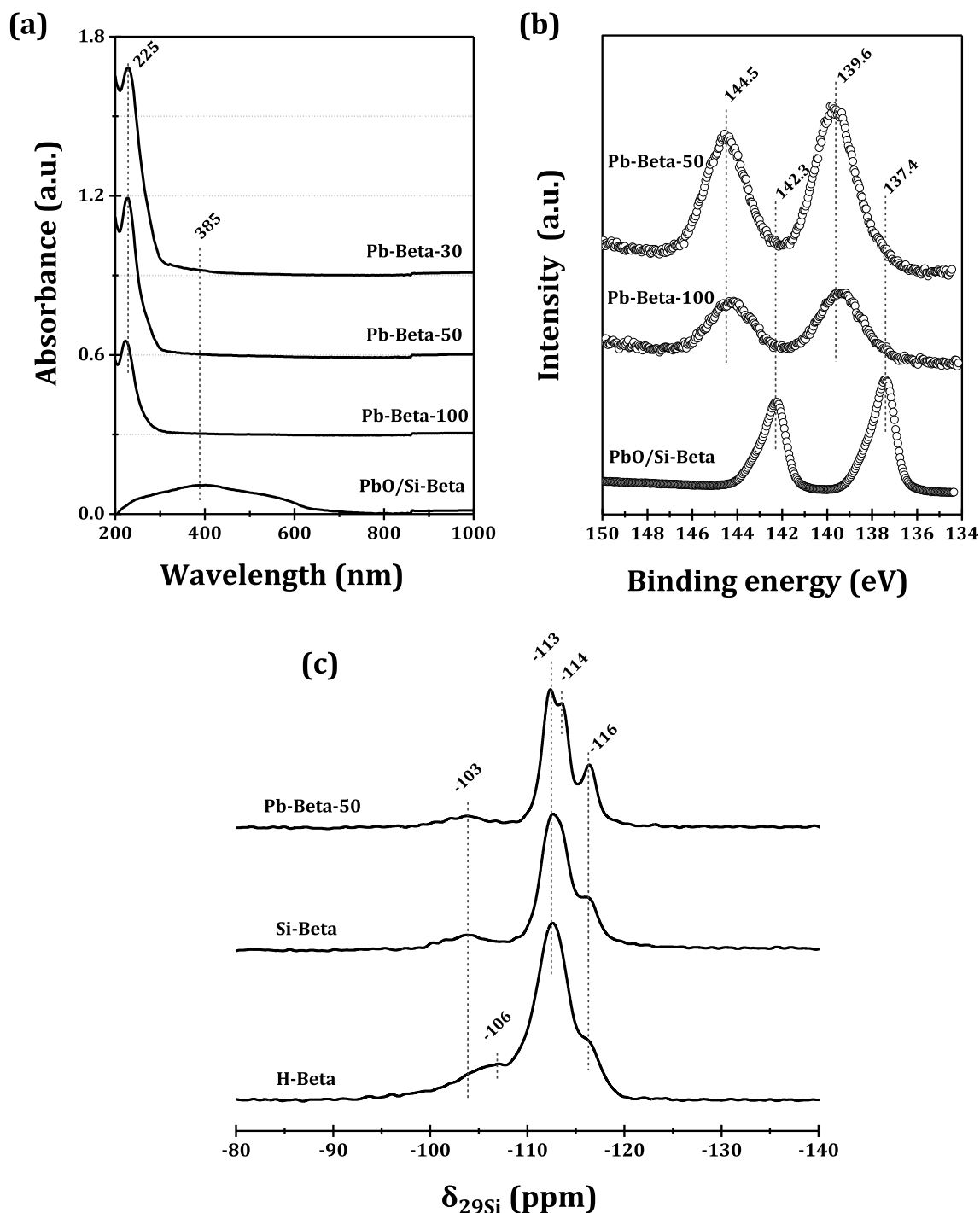


Fig. 5. (a) UV-vis spectra of Pb-containing samples. (b) Pb 4f XPS of Pb-Beta-50, Pb-Beta-100, and PbO/Si-Beta. (c) ^{29}Si MAS NMR spectra of selected zeolite samples.

atoms into Si-Beta leads to a significant decline in the intensities of isolated and associated Si-OH groups at 3740 and 3525 cm^{-1} , respectively [27]. According to the results from infrared spectroscopy, we conclude that Pb atoms have been successfully incorporated into the framework of Si-Beta zeolite via post-synthesis and probably exist in open configurations.

Notably, as shown in Fig. 3, the ionic radius of outsize Pb^{2+} (1.2 \AA , we will provide evidence on the formation of Pb^{2+} in the next section) is much larger than the prior Al^{3+} (0.54 \AA), and, theoretically, the Pb^{2+} is almost impossible to be fully incorporated into the vacant T sites of dealuminated Beta zeolite to generate closed sites $[\text{Pb}(\text{OSi})_4]$, being different to the cases of Ti-Beta, Sn-Beta and Zr-Beta where the ionic

radius of these metal ions are not so high compared to Al^{3+} [40]. On the other hand, according to the previous reports, the full-incorporation metal ions in close sites are generally accompanied with the detectable spacing increases in the position of the diffraction peak (302) at $2\theta = 22.6^\circ$ with respect to the diffraction of Si-Beta, which means the expansion of BEA framework due to the insertion of metal ions [27,41,42]. Here, after the incorporation of Pb ions, no obvious changes are detected in the d_{302} spacing ($2\theta = 22.6^\circ$, Fig. 1), roughly ruling out the formation of close sites $[\text{Pb}(\text{OSi})_4]$ [43]. Hence, as illustrated in Scheme 1, the wide-open site structure of $[\text{Pb}(\text{OSi})_2(\text{H}_2\text{O})_2]$ or $[\text{Pb}(\text{OSi})(\text{OH})(\text{H}_2\text{O})_2]$ is created in Pb-Beta zeolite [40].

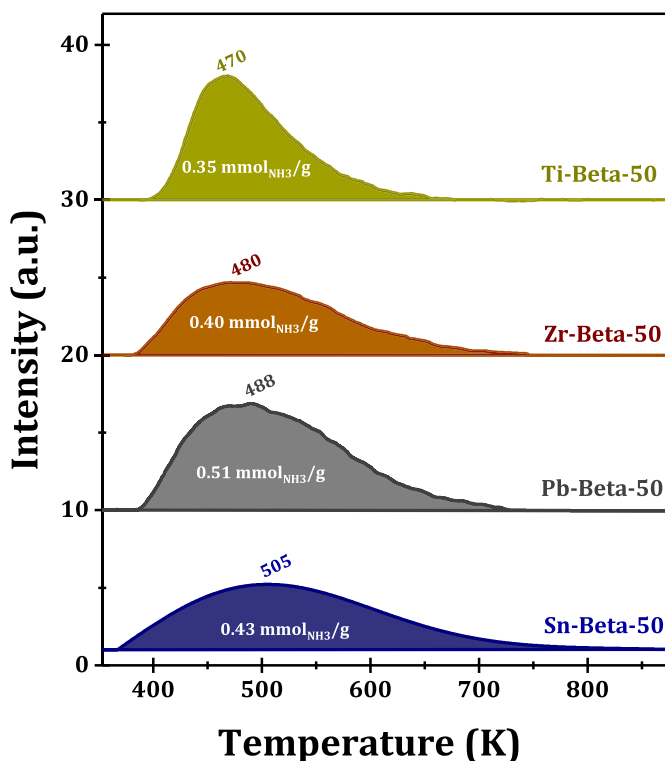


Fig. 6. NH_3 -TPD profiles of Ti-Beta-50, Zr-Beta-50, Pb-Beta-50, and Sn-Beta-50 with corresponding Lewis acid site density shown inside.

3.2. Existing state of Pb species in Pb-Beta

The existing state of Pb species in Pb-Beta can be directly observed by scanning transmission electron microscopy (STEM). As shown in the high-resolution high-angle annular dark-field (HAADF) STEM image (Fig. 4), the regular lattice fringes of Pb-Beta-50 zeolite can be clearly observed, corresponding to its high-crystallinity framework as revealed by XRD and TEM analysis. Meanwhile, even though few large-size bright spots can be observed (since TEM displays the two-dimensional projection of 3D images, large-size bright spots do not necessarily indicate the formation of large clusters), the HAADF-STEM image displays the majority of ultra-dispersed brighter spots rightly on the lattice fringes, which can be assigned to the heavier Pb atoms in the zeolite framework. Noticeably, some framework Pb single atoms are circled in yellow for a direct view. The corresponding element mapping analysis of random area in Pb-Beta-50 further indicates the ultra-dispersed state of Pb single atoms. In addition, the similar results of Pb-Beta-100 were shown in Fig. S4. In contrast, bright flecks with diameters of 2–3 nm due to PbO nanoparticles are clearly detected in the STEM image of PbO/Si-Beta (Fig. S5).

In order to further evaluate the existing states of the incorporated Pb atoms in the zeolite framework, diffuse reflectance UV-vis analysis is performed with dehydrated Pb-Beta zeolites and the corresponding spectra are shown in Fig. 5a. Pb-Beta samples with different Pb loadings essentially exhibit similar intense bands centered at 225 nm ascribed to the ligand-to-metal charge transfer from O^{2-} to Pb^{2+} (Si-O- as ligand), in analogy with Pb^{2+} (IV) complexes (i.e. Pb-N, Pb-S) [44,45]. Similar to the cases of other M-beta zeolites, e.g. Ti, Zr and Sn-Beta

Table 2
Aminolysis of ECH with aniline over various zeolite catalysts^a.

Entry	Catalyst	ECH conv.(%)	β -Amino alcohol select. (%)		TOF ^b (h^{-1})
			A	B	
1	H-Beta	< 5%	83	17	/
2	Si-Beta	6.7	95	5	/
3	Ti-Beta-50	63.4	92.2	7.8	1470
4	Zr-Beta-50	73.5	93.5	6.5	1714
5	Sn-Beta-50	43.0	90.7	9.3	1002
6	Pb-Beta-50	81.8	94.3	5.7	1904
7	Pb-Beta-100	42.6	93.6	6.4	1986
8	Pb-Beta-30	69.7	94.8	5.2	812
9	PbO/Si-Beta	9.6	94.5	5.5	/

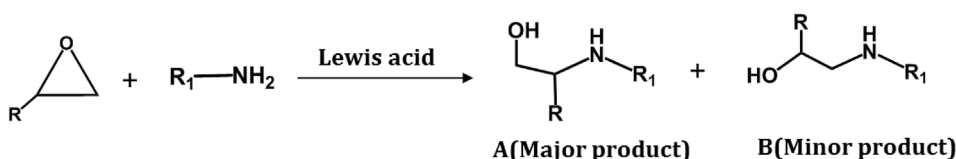
^a Reaction conditions: 10 mmol epoxide, 10 mmol aniline, 25 mg catalyst, temperature = 313 K, reaction time = 0.5 h.

^b Calculated as the number of moles of epoxide converted per mole of the metal center per hour.

[26,27,46,47], the UV band in 200–250 region is generally assumed to be the isolated tetrahedrally coordinated atoms in the zeolite framework. Compared to closed M sites $[\text{M}(\text{OSi})_4]$ in the framework of Ti-Beta (210 nm), Zr-Beta (205 nm) and Sn-Beta (207 nm), noticeable shift of Pb-Beta toward higher wavelength band is observed, probably due to the formation of wide-open Pb (IV) structures $[\text{Pb}(\text{OSi})_n(\text{OH})_{4-n}]$ in Pb-Beta zeolite [20,47]. In the case of PbO supported on Si-Beta, i.e. PbO/Si-Beta, a very broad band centered at ~ 385 nm is observed and attributed to the charge transfer from Pb-O-Pb bands [45,48]. For all Pb-Beta samples, only Pb-Beta-30 shows a very weak peak at ~ 385 nm, indicating the formation of a small quantity of PbO species at this high Pb loading.

The electronic states of Pb species in as-synthesized Pb-Beta zeolites are further investigated by XPS and the results are shown in Fig. 5b. The binding energy values of 139.6 and 144.5 eV corresponding to Pb $4f_{7/2}$ and $4f_{5/2}$, respectively, could be observed for the two Pb-Beta samples, which are greatly higher than the PbO/Si-Beta (137.4 and 142.3 eV corresponding to bulk PbO reference). Due to the lower electronegativity of Pb compared to Si atom, the shifts towards higher values indicate that the incorporated Pb ions into zeolite framework are more positively charged in Pb-O-Si bands than Pb-O-Pb bands of bulk PbO. Moreover, based on the framework metal species in literature reports (45), this higher shift should be ascribed to the change in geometry from octahedral to tetrahedral-coordination, in agreement with the results UV-vis spectroscopy. This is further confirmed by Raman analysis where no Raman active modes corresponding to PbO [49] can be detected in post-synthesized Pb-Beta (Fig. S6).

For a better understanding the local environment of Pb species in Beta zeolites, the ^{29}Si MAS NMR spectra was performed (Fig. 5c). The parent H-beta shows a series characteristic signals [46,50]: $\text{Si}(\text{OSi})_4$ species (Q^4 , -116 and -113 ppm corresponding to different crystallographic sites), $\text{Si}(\text{OSi})_3(\text{OAl})$ groups (Q^4 , -106 ppm), $\text{Si}(\text{OSi})_3(\text{OH})$ groups (SiOH , Q^3 , -103 ppm). As a result of the dealumination, the signal caused by $\text{Si}(\text{OSi})_3(\text{OAl})$ species disappeared, demonstrating the removal of framework Al atoms. The intensities of signals due to $\text{Si}(\text{OSi})_4$ species (Q^4) remain nearly unchanged, while the intensities of the signal due to $\text{Si}(\text{OSi})_3(\text{OH})$ groups (Q^3) increases obviously, indicating the changes of the SiOH defect sites in the Beta zeolite. Significantly, compared to conventional M-Beta zeolites (such as Ti-Beta) with closed Ti sites [46], the incorporation of Pb atoms into Si-Beta



Scheme 2. Ring-opening of epoxides with amines catalyzed by solid Lewis acids.

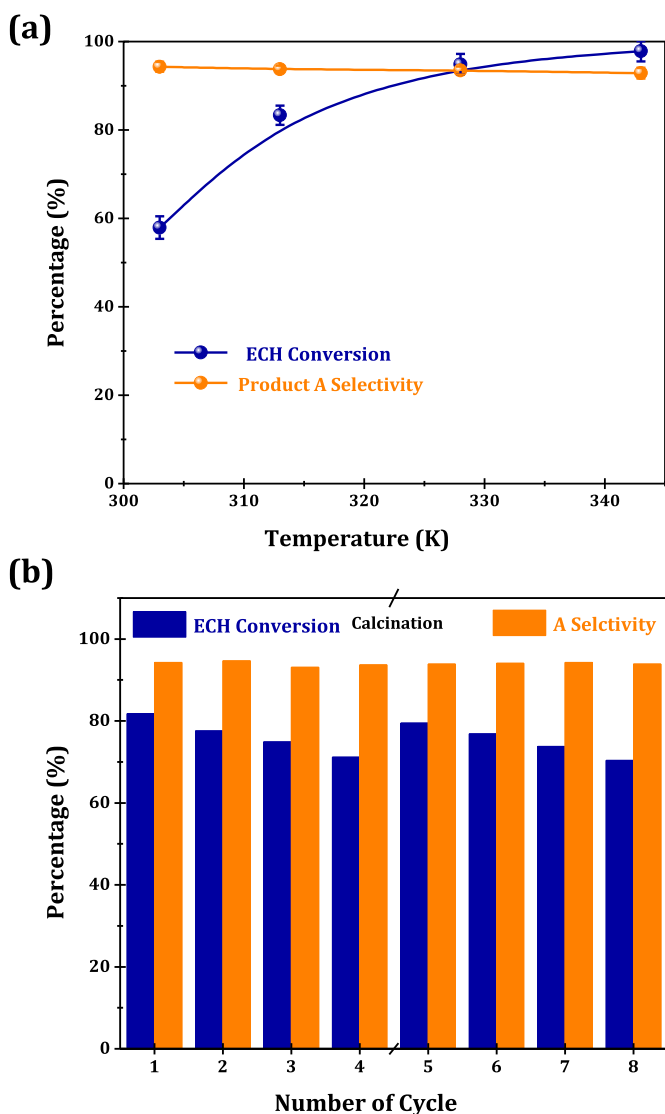


Fig. 7. (a) Aminolysis of ECH with aniline over Pb-Beta-50 at different temperatures. Reaction conditions: 10 mmol ECH, 10 mmol aniline, 25 mg catalyst, time = 0.5 h. (b) Recycling test for the ring-opening aminolysis of ECH with aniline catalyzed by Pb-Beta-50. Reaction conditions: 10 mmol ECH, 10 mmol aniline, 25 mg catalyst, temperature = 313 K, time = 0.5 h. Calcination conditions: 723 K in flowing air for 4 h.

framework causes distinct changes at the Q^4 silicon species, with a significant increase at -116 ppm and the appearance of a new split signal at -114 ppm, indicating the strong interaction between Pb species and Si-Beta framework. The wide-open heavy Pb-atom sites in SiO-Pb-OH groups should be responsible for the changes in the ^{29}Si MAS NMR spectra of Pb-Beta zeolite.

According to the characterization results from HAADF-STEM, UV-vis, XPS, and ^{29}Si MAS NMR, most Pb single atoms have been successfully incorporated into the Beta framework through the post-synthesis modifications and exist as isolated tetrahedral Pb with open configurations. Compared with previous M-Beta (Ti-, Zr-, and Sn-Beta) zeolites in literature reports, the wide-open Pb structures (in Pb-Beta) generated from the outsize heavy Pb atom bring about significant changes in spectroscopic characterization results.

3.3. Acidic properties of Pb-Beta

The type and density of acidic sites of Pb-beta zeolites and reference samples are evaluated by means of NH_3 -TPD. As shown in Fig. S7, parent H-Beta zeolite demonstrates a wider temperature range of NH_3

desorption from 353 to 873 K, and two desorption peaks centered at 505 and 660 K reveal the presence of both weak and strong acid sites, respectively. After the dealumination of H-Beta, no desorption peaks can be observed for the resulting Si-Beta sample since it is free of any acid sites (Fig. S8). Subsequently, the incorporation of metal ions (i.e. Ti^{4+} , Zr^{4+} , and Sn^{4+}) into Beta framework could create some Lewis acid sites, as confirmed by the NH_3 -TPD peaks at 470–505 K (Fig. 6), which are also evidenced by FTIR spectra of pyridine adsorption in our previous works [26,27,45]. Concretely, the strength of Lewis acidity could be determined as Sn-Beta (505 K) > Zr-Beta (480 K) > Ti-Beta (470 K), consistent with previous reported studies and theoretical predictions [24,25,51]. The NH_3 desorption peak centered at 488 K was observed in the Pb-Beta zeolite, which was similar to the desorption temperature of Zr-Beta, with moderate Lewis acidic strength.

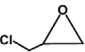
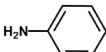
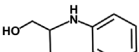
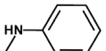
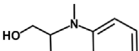
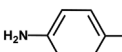
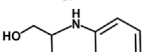
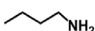
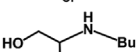

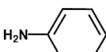
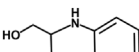
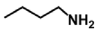
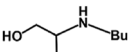
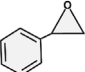
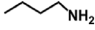
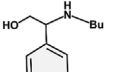
For a better comparison of these Lewis acidic samples, a quantitative analysis on the Lewis acid site density measured by NH_3 -TPD are performed (Fig. 6, Table S1). The Lewis acidic density is obtained in the sequence of Pb-Beta-50 (0.51 mmol g^{-1}) > Sn-Beta-50 (0.43 mmol g^{-1}) > Zr-Beta-50 (0.40 mmol g^{-1}) > Ti-Beta-50 (0.35 mmol g^{-1}), indicating that more Lewis acid sites are created via Pb incorporation. Since a Lewis acid site is essentially generated from a M-OH group, the overabundant Lewis acid sites ($n_{\text{NH}_3}/n_{\text{Pb}} = 1.64$) clearly disclose the presence of wide-open Pb sites (SiO-Pb-OH groups) in Pb-Beta zeolite, while the slightly different Lewis acidic densities of other three M-Beta zeolites are probably due to the subtle distinction of metals coordinating properties. Significantly, the sufficient active Lewis acid sites created from open Pb sites in Pb-Beta zeolites should improve their catalytic efficiency in the chemical processes.

3.4. Catalytic properties of Pb-Beta in the aminolysis of epoxides

The catalytic performance of as-prepared Pb-Beta, together with some other M-Beta samples for reference, is thoroughly investigated in the ring-opening reaction of epoxide with aniline to yield two regioisomer β -amino alcohol products, i.e. major product A and minor product B (Scheme 2). Firstly, epichlorohydrin (ECH) and aniline were chosen as representative epoxide and amine, respectively. Under our reaction conditions, the aminolysis of ECH by aniline does not proceed without a catalyst (not shown) and negligible products (< 7.2%) are obtained in the presence of H-Beta or Si-Beta as a catalyst (Table 2, Entry 1&2). Pb-Beta zeolite (Entry 6) showed higher catalytic activity (in terms of turnover frequency, TOF) than bulk PbO species (PbO/Si-Beta, Entry 9), indicating that framework-incorporated Pb species are the optimized active components for this reaction. The TOF values of different M-beta Lewis acid catalysts are observed in the order of Pb-Beta-50 > Zr-Beta-50 > Ti-Beta-50 > Sn-Beta-50 (Entry 3-5). The strong adsorption for amines over Sn-beta with highest Lewis acidic strength will hinder the adsorption for epoxides, while the Ti-Beta with lowest Lewis acidic strength cannot efficiently activate the epoxides substrate for a minolysis reaction. Despite that Zr-Beta with moderate Lewis acidic strength exhibits high activity for the reaction, the much more abundant active sites generated from the unique wide-open Pb sites of Pb-Beta can lead to a higher catalytic activity. These results clearly demonstrate that Pb-Beta-50 is an excellent catalyst for the aminolysis of epoxides, comparable with the best results ever reported (Table S2).

As shown in Table 2 (Entry 6-8), Pb-Beta-30 with highest Pb loading exhibits lower activity (TOF = 812 h^{-1}) in the reaction, while the similar high activity could be observed for Pb-Beta-50 (TOF = 1904 h^{-1}) and Pb-Beta-100 (TOF = 1986 h^{-1}). We suppose that the approaching saturation of framework Pb in Beta zeolite at $n_{\text{Si}}/n_{\text{Pb}}$ of 50 and more Pb species tend to form oxides covering the framework Pb atoms and therefore lead to low catalytic activity. To confirm this speculation, microscopy analysis and NH_3 -TPD were further performed. For Pb-Beta-30 sample, PbO nanoparticles of 2–3 nm were clearly detected in TEM (Fig. S9 left) and HAADF-STEM image (red circles, Fig. S9 right), even well-isolated Pb atoms (yellow circles) can be observed as well. In

Table 3
Aminolysis of epoxides with amines over Pb-Beta-50 catalyst^a.

Epoxide	Amine	β -Amino alcohol	Epoxide Conv.(%)	β -Amino alcohol Select.(%)	TOF ^b (h ⁻¹)
			81.8	94.3	1904
			69.1	91.8	1608
			73.2	92.4	1704
			42.3	74.5	984
			65.6	95.1	1526
			40.7	71.1	946
			39.5	68.8	918

^a Reaction conditions: 10 mmol epoxide, 10 mmol amine, 25 mg catalyst, temperature = 313 K, reaction time = 0.5 h.

^b Calculated as the number of moles of epoxide converted per mole of the metal center per hour.

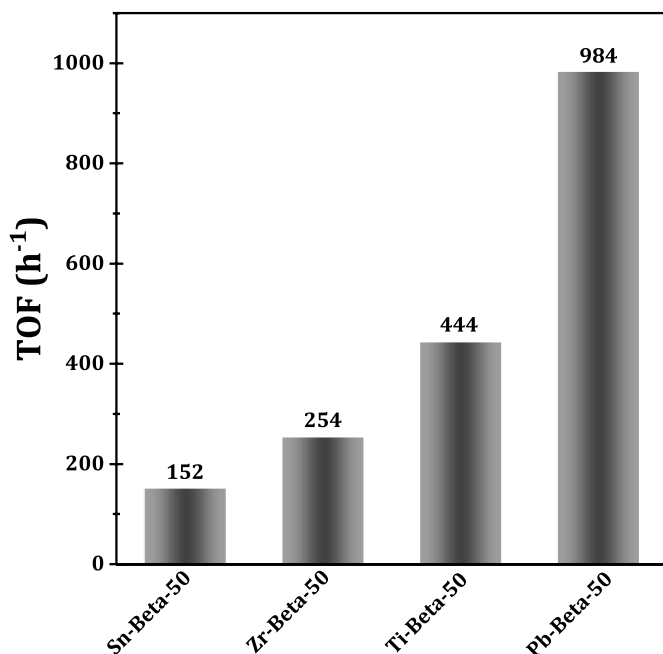


Fig. 8. Catalytic activity of ECH aminolysis with butylamine over various M-Beta zeolites.

addition, the Lewis acidic density, as calculated from NH₃-TPD analysis (Fig. S8), could be in the order of Pb-Beta-50 (0.51 mmol g⁻¹) > Pb-Beta-30 (0.45 mmol g⁻¹) > Pb-Beta-100 (0.27 mmol g⁻¹), strongly indicating the presence of significant amount of PbO species located in the nonframework positions of Pb-Beta-30 zeolite, which cannot generate Lewis acid sites and, therefore, lead to lower catalytic activity.

Fig. 7 (left) shows the influence of temperature on the conversion and product selectivity over Pb-Beta-50 in the aminolysis of ECH in 0.5 h. As the temperature increases from 303 to 343 K, the conversion of ECH in 0.5 h could increase from 56.1 to 96.2%, and there is a marginal decrease in the product selectivity (by ~2%) indicating that at higher conversion part of A got isomerized into B. Furthermore, under such

Table 4
Competitive adsorption of ECH and butylamine on M-Beta samples^a.

Catalyst	Substrate adsorbed (mmol g _{zeolite} ⁻¹)			ECH/ Butylamine	ECH conv. (%) ^b
	ECH	Butylamine	Total		
Pb-Beta-50	0.11	0.18	0.29	0.61	42.3
Sn-Beta-50	0.03	0.21	0.24	0.14	6.5
Zr-Beta-50	0.05	0.17	0.22	0.29	10.9
Ti-Beta-50	0.06	0.13	0.19	0.46	19.1

^a 50 mg of the zeolite was suspended for 0.5 h with equimolar amounts (2 mmol) of epichlorohydrin (ECH) and butylamine dissolved in 5 mL of CH₂Cl₂. The catalyst, then, was separated and the concentration of the substrate in the liquid portion was determined by gas chromatography. The amount adsorbed on the catalyst surface was determined by substrate concentration difference.

^b ECH conversion was obtained at 313 K after a reaction time of 0.5 h.

mild reaction conditions, the Pb-Beta catalyst exhibited stable activity and regenerated property even after eight successive recycles (Fig. 7 right), and the structural collapse and possible leaching of Pb species after recycle experiments can be excluded by XRD diffraction (Fig. S10) and XRF analysis (Table S3), respectively. These results clearly demonstrate the Pb-Beta zeolite was a robust catalyst for the aminolysis of epoxides.

In order to further demonstrate the versatility of Pb-Beta Lewis acidic catalyst in the aminolysis of epoxides, the substrate scope was broadened by varying the epoxide and amine reactants. As shown in Table 3, high activity for the β -amino alcohol products could be obtained for most substrates of different epoxides and amines. In addition, the reactivity of amines could influence the epoxides conversion, with activity decreasing in the following sequence: aniline > substituted anilines > butylamine. The very low activity in the aminolysis of epoxides with butylamine has been observed using Ti-containing zeolites [32,33], Zr-Beta [26] or Zr-MFI [34] as catalysts. As shown in Table S2 (Entry 8-12), it is still challenging to obtain adequate aminolysis activity when using butylamine as the substrate. As proposed in these literature, this trend can be generally explained from the pK_a value (Fig. S11), i.e. the basicity of amines, and the adsorption ability of reactant molecules. For most amine substrates, there is a good correlation

between pK_a of amine with catalytic activity. That is, the catalytic activity decreases with increasing basicity (pK_a) of the amine. For a catalyst to exhibit high catalytic activity, there should be an optimum bonding between the catalyst active sites and reactant molecules. Therefore, if the high-basicity amine, e.g. butylamine, is strongly bonded with Lewis acid sites in conventional M-Beta (Ti-, Zr-, and Sn-Beta), the amine adsorbed sites will not be available to activate epoxide for the ring-opening reaction. We then come back to the performance of the aminolysis of epoxides with butylamine over the Pb-Beta catalyst with unique wide-open Pb sites (Table 3). Significantly, although there was no as high as TOF value like other amines with lower basicity, much higher catalytic activity of Pb-Beta sample in this reaction was obtained compared with traditional M-Beta zeolites (Fig. 8) or other solid acidic materials (Table S2, Entry 8–12).

According to the distinct activity of Pb-Beta catalyst, we conclude that the adsorption of epoxide in the condition of high-basicity butylamine is an important factor for the ring-opening of epoxide. To confirm our hypothesis, competitive adsorption experiments of ECH and butylamine were performed with catalysts under study, as shown in Table 4. As expected, Pb-Beta-50 zeolite, with highest ECH/butylamine adsorption ratio of 0.61, exhibited the best catalytic performance with regard to aminolysis reaction rate, followed by Ti-Beta-50 (0.46), Zr-Beta-50 (0.29), Sn-Beta-50 (0.14). On the other hand, the highest total adsorption amount of both substrates over Pb-Beta-50 zeolite was also demonstrated in Table 4. These comparative data clearly indicate that the adsorption of epoxide in Pb-Beta zeolite is not seriously affected with the co-existence of high-basicity butylamine, due to its unique wide-open Pb sites.

4. Conclusion

In summary, outside Pb atoms have been successfully incorporated into the framework of Beta zeolite via a simple post-synthesis strategy with the combination of complete dealumination and subsequent dry impregnation of Pb precursor. Characterization results from HAADF-STEM, UV-vis, XPS, and ^{29}Si MAS NMR spectroscopy reveal that most incorporated Pb species exist in the form of well isolated tetrahedral Pb ions in the BEA framework with open configurations. The as-prepared Pb-Beta zeolites are identified as versatile solid Lewis acid that exhibit remarkable catalytic in the ring-opening aminolysis of epoxides to produce β -amino alcohols, outperforming traditional Lewis acidic Ti-, Zr-, and Sn-zeolites. The superior activity of Pb-Beta zeolites can be explained by the abundant Lewis acid sites with moderate acidic strength created from unique wide-open Pb sites.

This work presents a first example of incorporating outside heteroatoms into zeolite framework via a post-synthesis strategy to create wide-open Lewis acid sites for catalytic applications. It also demonstrates that Pb can become an active component rather than a deactivation component or a modifier by careful tuning its existing state within zeolite matrix.

Acknowledgements

This work was supported by the National Natural Science Foundation of China (21573113, 21421001), Municipal Natural Science Foundation of Tianjin (16JQJNC04900) and Sinopec Corp. (417012-2).

Appendix A. Supplementary data

Supplementary data related to this article can be found at <http://dx.doi.org/10.1016/j.micromeso.2018.01.033>.

References

- [1] M.S. Holm, S. Saravanamurugan, E. Taarning, Conversion of sugars to lactic acid

- derivatives using heterogeneous zeotype catalysts, *Science* 328 (2010) 602–605.
- [2] K. Yakabi, T. Mathieux, K. Milne, E.M. López-Vidal, A. Buchard, C. Hammond, Continuous production of biorenewable, polymer-grade lactone monomers through Sn- β -catalyzed Baeyer–Villiger oxidation with H_2O_2 , *ChemSusChem* 10 (2017) 3652–3659.
- [3] Z. Zhu, H. Xu, J. Jiang, Y. Guan, P. Wu, Sn-Beta zeolite hydrothermally synthesized via interzeolite transformation as efficient Lewis acid catalyst, *J. Catal.* 352 (2017) 1–12.
- [4] M. Moliner, State of the art of Lewis acid-containing zeolites: lessons from fine chemistry to new biomass transformation processes, *Dalton Trans.* 43 (2014) 4197–4208.
- [5] A. Corma, L.T. Nemeth, M. Renz, S. Valencia, Sn-zeolite beta as a heterogeneous chemoselective catalyst for Baeyer–Villiger oxidations, *Nature* 412 (2001) 423–425.
- [6] Y. Román-Leshkov, M.E. Davis, Activation of carbonyl-containing molecules with solid Lewis acids in aqueous media, *ACS Catal.* 1 (2011) 1566–1580.
- [7] S. Valencia, A. Corma, U.S. Patent 5, 968, 473A, October 19, 1999.
- [8] C. Paris, M. Moliner, A. Corma, Metal-containing zeolites as efficient catalysts for the transformation of highly valuable chiral biomass-derived products, *Green Chem.* 15 (2013) 2101.
- [9] P. Li, G. Liu, H. Wu, Y. Liu, J.-G. Jiang, P. Wu, Postsynthesis and selective oxidation properties of nanosized Sn-Beta zeolite, *J. Phys. Chem. C* 115 (2011) 3663–3670.
- [10] C. Hammond, S. Conrad, I. Hermans, Simple and scalable preparation of highly active Lewis acidic Sn- β , *Angew. Chem. Int. Ed.* 51 (2012) 11736–11739.
- [11] A. Al-Nayili, K. Yakabi, C. Hammond, Hierarchically porous BEA stannosilicates as unique catalysts for bulky ketone conversion and continuous operation, *J. Mater. Chem. A* 4 (2016) 1373–1382.
- [12] B.D. Montejo-Valencia, M.C. Curet-Arana, DFT study of the Lewis acidities and relative hydrothermal stabilities of BEC and BEA zeolites substituted with Ti, Sn, and Ge, *J. Phys. Chem. C* 119 (2015) 4148–4157.
- [13] X. Ouyang, S.-J. Hwang, D. Xie, T. Rea, S.I. Zones, A. Katz, Heteroatom-substituted delaminated zeolites as solid Lewis acid catalysts, *ACS Catal.* 5 (2015) 3108–3119.
- [14] T. Salavati-fard, S. Caratzoulas, R.F. Lobo, D.J. Doren, Catalysis of the Diels–Alder reaction of furan and methyl acrylate in Lewis acidic zeolites, *ACS Catal.* 7 (2017) 2240–2246.
- [15] J.W. Harris, M.J. Cordon, J.R. Di Iorio, J.C. Vega-Vila, F.H. Ribeiro, R. Gounder, Titration and quantification of open and closed Lewis acid sites in Sn-Beta zeolites that catalyze glucose isomerization, *J. Catal.* 335 (2016) 141–154.
- [16] G. Yang, L. Zhou, X. Han, Lewis and Brønsted acidic sites in M^{4+} -doped zeolites (M = Ti, Zr, Ge, Sn, Pb) as well as interactions with probe molecules: a DFT study, *J. Mol. Catal. A* 363–364 (2012) 371–379.
- [17] M. Boronat, A. Corma, M. Renz, P.M. Viruela, Predicting the activity of single isolated Lewis acid sites in solid catalysts, *Chem. Eur. J.* 12 (2006) 7067–7077.
- [18] M. Boronat, P. Concepcion, A. Corma, M. Renz, S. Valencia, Determination of the catalytically active oxidation Lewis acid sites in Sn-beta zeolites, and their optimisation by the combination of theoretical and experimental studies, *J. Catal.* 234 (2005) 111–118.
- [19] V. L. Sushkevich, A. Vimont, A. Travert, I. I. Ivanova, Spectroscopic evidence for open and closed Lewis acid sites in ZrBEA zeolites, *J. Phys. Chem. C* 119, 17633–17639.
- [20] P. Ratnasamy, D. Srinivas, H. Knözinger, Active sites and reactive intermediates in titanium silicate molecular sieves, *Adv. Catal.* 48 (2004) 1–169.
- [21] D.H. Wells, W.N. Delgass, K.T. Thomson, Evidence of defect-promoted reactivity for epoxidation of propylene in titanosilicate (TS-1) catalysts: a DFT study, *J. Am. Chem. Soc.* 126 (2004) 2956–2962.
- [22] S. Bordiga, F. Bonino, A. Damin, C. Lamberti, Resonance Raman effects in TS-1: the structure of Ti(IV) species and reactivity towards H_2O , NH_3 and H_2O_2 : an in situ study, *Phys. Chem. Chem. Phys.* 9 (2007) 4854–4878.
- [23] V.L. Sushkevich, D. Palagin, I.I. Ivanova, With open arms: open sites of ZrBEA zeolite facilitate selective synthesis of butadiene from ethanol, *ACS Catal.* 5 (2015) 4833–4836.
- [24] A. Corma, M. E. Domine, L. Nemeth, S. Valencia, Al-free Sn-Beta zeolite as a catalyst for the selective reduction of carbonyl compounds (Meerwein–Ponndorf–Verley reaction), *J. Am. Chem. Soc.* 124, 3194–3195.
- [25] A. Corma, Water-resistant solid Lewis acid catalysts: Meerwein–Ponndorf–Verley and Oppenauer reactions catalyzed by tin-beta zeolite, *J. Catal.* 215 (2003) 294–304.
- [26] B. Tang, W. Dai, X. Sun, G. Wu, N. Guan, M. Hunger, L. Li, Mesoporous Zr-Beta zeolites prepared by a post-synthetic strategy as a robust Lewis acid catalyst for the ring-opening aminolysis of epoxides, *Green Chem.* 17 (2015) 1744–1755.
- [27] B. Tang, W. Dai, G. Wu, N. Guan, L. Li, M. Hunger, Improved post-synthesis strategy to Sn-Beta zeolites as Lewis acid catalysts for the ring-opening hydration of epoxides, *ACS Catal.* 4 (2014) 2801–2810.
- [28] V.L. Sushkevich, I.I. Ivanova, S. Tolborg, E. Taarning, Predicting the activity of single isolated Lewis acid sites in solid catalysts, *J. Catal.* 316 (2014) 121–129.
- [29] T. De Baerdemaeker, B. Steenackers, D. De Vos, Ti-substituted zeolite Beta: a milestone in the design of large pore oxidation catalysts, *Chem. Commun* 49 (2013) 7474–7476.
- [30] D.J. Ager, I. Prakash, D.R. Schaad, 1,2-Amino alcohols and their heterocyclic derivatives as chiral auxiliaries in asymmetric synthesis, *Chem. Rev.* 96 (1996) 835–876.
- [31] P. O'Brien, Sharpless asymmetric aminohydroxylation: scope, limitations, and use in synthesis, *Angew. Chem. Int. Ed.* 38 (1999) 326–329.
- [32] L. Saikia, J. Satyarthi, D. Srinivas, P. Ratnasamy, Activation and reactivity of epoxides on solid acid catalysts, *J. Catal.* 252 (2007) 148–160.
- [33] A. Kumar, D. Srinivas, Aminolysis of epoxides catalyzed by three-dimensional, mesoporous titanosilicates, Ti-SBA-12 and Ti-SBA-16, *J. Catal.* 293 (2012)

- 126–140.
- [34] R. Kore, R. Srivastava, B. Satpati, Highly efficient nanocrystalline zirconosilicate catalysts for the aminolysis, alcoholysis, and hydroamination reactions, *ACS Catal.* 3 (2013) 2891–2904.
- [35] S. Song, L. Di, G. Wu, W. Dai, N. Guan, L. Li, Meso-Zr-Al-beta zeolite as a robust catalyst for cascade reactions in biomass valorization, *Appl. Catal.*, B 205 (2017) 393–403.
- [36] G.G. Juttu, R.F. Lobo, Framework modification of microporous silicates via gas-phase treatment with $ZrCl_4$, *Catal. Lett.* 62 (1999) 99–106.
- [37] T.D. Courtney, C.-C. Chang, R.J. Gorte, R.F. Lobo, W. Fan, V. Nikolakis, Effect of water treatment on Sn-BEA zeolite: origin of 960 cm^{-1} FTIR peak, *Microporous Mesoporous Mater.* 210 (2015) 69–76.
- [38] M.A. Cambor, A. Corma, A. Martinez, J. Pérez-Pariente, Infrared spectroscopic investigation of titanium in zeolites. A new assignment of the 960 cm^{-1} band, *J. Chem. Soc. Chem. Commun.* (1993) 557–559.
- [39] J.-P. Nogier, Y. Millot, P.P. Man, T. Shishido, M. Che, S. Dzwigaj, Probing the incorporation of Ti(IV) into the BEA zeolite framework by XRD, FTIR, NMR, and DR UV-vis, *J. Phys. Chem. C* 113 (2009) 4885–4889.
- [40] S. Dzwigaj, Y. Millot, J.-M. Krafft, N. Popovych, P. Kyriienko, Incorporation of silver atoms into the vacant T-atom sites of the framework of SiBEA zeolite as mononuclear Ag(I) evidenced by XRD, FTIR, NMR, DR UV-vis, XPS, and TPR, *J. Phys. Chem. C* 117 (2013) 12552–12559.
- [41] S. Dzwigaj, J. Janas, J. Gurgul, R.P. Socha, T. Shishido, M. Che, Do Cu(II) ions need Al atoms in their environment to make CuSiBEA active in the SCR of NO by ethanol or propane? A spectroscopy and catalysis study, *Appl. Catal. B* 85 (2009) 131–138.
- [42] M.M.J. Treacy, J.M. Newsam, Two new three-dimensional twelve-ring zeolite frameworks of which zeolite beta is a disordered intergrowth, *Nature* 332 (1988) 249.
- [43] A. Rokicińska, M. Drozdek, B. Dudek, B. Gil, P. Michorczyk, D. Brouri, S. Dzwigaj, P. Kuśtrowski, Cobalt-containing BEA zeolite for catalytic combustion of toluene, *Appl. Catal.*, B 212 (2017) 59–67.
- [44] N.S. Sisombath, F. Jalilehvand, A.C. Schell, Q. Wu, Lead(II) binding to the chelating agent D-Penicillamine in aqueous solution, *Inorg. Chem.* 53 (2014) 12459–12468.
- [45] V. Hernández-Morales, R. Nava, Y.J. Acosta-Silva, S.A. Macías-Sánchez, J.J. Pérez-Bueno, B. Pawelec, Adsorption of lead (II) on SBA-15 mesoporous molecular sieve functionalized with $-NH_2$ groups, *Microporous Mesoporous Mater.* 160 (2012) 133–142.
- [46] B. Tang, W. Dai, X. Sun, N. Guan, L. Li, M. Hunger, A procedure for the preparation of Ti-Beta zeolites for catalytic epoxidation with hydrogen peroxide, *Green Chem.* 16 (2014) 2281–2291.
- [47] L. Xu, D.D. Huang, C.G. Li, X. Ji, S. Jin, Z. Feng, F. Xia, X. Li, F. Fan, C. Li, P. Wu, Construction of unique six-coordinated titanium species with an organic amine ligand in titanosilicate and their unprecedented high efficiency for alkene epoxidation, *Chem. Commun.* 51 (2015) 9010–9013.
- [48] X. Li, L. Gao, Y. Niu, C. Liu, G. Che, Y. Yan, Q. Guan, Pb(II) coordination polymer based on mixed ligands: syntheses, structures, photoluminescence, and photocatalysis, *J. Inorg. Organomet. Polym.* 25 (2015) 886–891.
- [49] J.P. Vigouroux, G. Calvarin, E. Husson, Etude vibrationnelle des oxydes $PbO\ \alpha$ et $PbO\ \beta$: interpretation en relation avec la dilatation thermique, *J. Solid State Chem.* 45 (1982) 343–352.
- [50] M. Hunger, S. Ernst, J. Weitkamp, Multinuclear solid-state NMR investigation of zeolite MCM-22, *Zeolites* 15 (1995) 188–192.
- [51] G. Yang, E.A. Pidko, E.J.M. Hensen, Structure, stability, and Lewis acidity of mono and double Ti, Zr, and Sn framework substitutions in BEA zeolites: a periodic density functional theory study, *J. Phys. Chem. C* 117 (2013) 3976–3986.